ACS APPLIED OPTICAL MATERIALS

pubs.acs.org/acsaom
Article

Harnessing Short-Range Surface Plasmons in Planar Silver Films via Disorder-Engineered Metasurfaces

Maximilian Buchmüller, Ivan Shutsko, Sven Oliver Schumacher, and Patrick Görrn*

Cite This: ACS Appl. Opt. Mater. 2023, 1, 1777−1782
Read Online

ABSTRACT: Short-range surface plasmon polaritons (SR-SPPs) can arise due to the hybridization of surface plasmon polaritons propagating along the two interfaces of a thin metal slab. In optics, they have gained particular interest for imaging and sensing applications because of their short wavelengths at optical frequencies along with strong field enhancement. However, mediating the interaction of SR-SPPs with photons in planar films is difficult because of the large momentum mismatch. For efficient coupling, nanostructuring such thin films (~20 nm thickness), or placing metallic nanostructures in close proximity to the planar film, is technologically challenging and can strongly influence the SR-SPP properties. In this article, harnessing SR-SPPs in planar silver films is demonstrated using disorder-engineered metasurfaces. Disorder-engineering is realized by the light-controlled growth of silver nanoparticles. The dispersion of the hybrid modes with the silver thickness is measured and compared with simulations. We anticipate these results to introduce a facile method for harnessing SR-SPPs in planar optical systems and make use of their promising properties for imaging, sensing, and nonlinear optics.

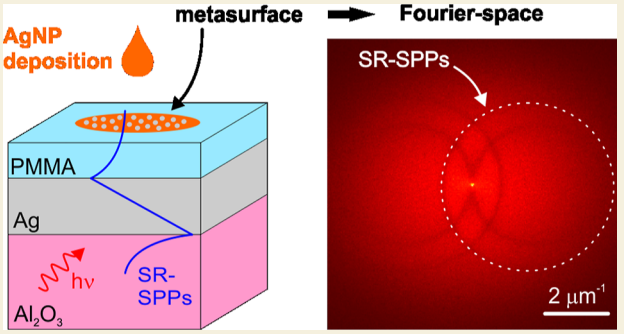

KEYWORDS: *short-range surface plasmons, plasmonic nanoparticles, engineered disorder, metasurfaces, plasmonics, tailored disorder*

1. INTRODUCTION

Surface plasmon polaritons (SPPs) are electromagnetic surface waves propagating along a metal/dielectric interface, which can be excited by the coupling of photons to collective oscillations of free electrons in the metal.[1] Perpendicular to the interface, SPPs are confined evanescently on subwavelength scales, while their propagation length is governed by radiation loss and absorption loss inside the metal.[2] Due to their strong field confinement beyond the optical diffraction limit, SPPs enable immense electromagnetic field enhancement inside nanoscale mode volumes.[3] As a result, SPPs have gained remarkable attention in modern optics with a wide range of applications, including surface-enhanced Raman spectroscopy,[4,5] nonlinear optics,[6] and sensing.[7]

In many of these applications, noble metal (e.g., silver) films are used together with other functional layers in a planar stack geometry. Such planar metal films support two surface plasmon modes, one at each interface of the film. For large film thicknesses of the metal t_m, the two SPPs can be treated as individual single-interface surface plasmons with wavevectors governed by the respective permittivity profiles adjacent to each interface. If the metal film becomes sufficiently thin (t_m on the order of a few tens of nanometers), the two SPP modes can hybridize. This hybridization can be described by a coupled system with two eigenmodes, showing dispersion with the film thickness t_m.[8] While one eigenmode extends far into the dielectric, the other eigenmode is strongly confined to the metal slab and thus possesses significantly higher absorption loss. Therefore, the two eigenmodes are often referred to as long-range (LR) and short-range (SR) surface plasmons because of their comparatively long and short propagation lengths, respectively.

Given their strong field enhancement and short wavelengths, SR-SPPs have been used for sensing,[9] focusing,[10,11] and high-resolution microscopy.[12] The formation of hybrid bound states in the continuum (BICs) has also been investigated recently when SR-SPPs are coupled to photonic waveguide modes.[13] Although being of high interest, SR-SPPs have received less attention compared to LR-SPPs in the past.[14] On the one hand, SR-SPPs are relatively difficult to address with photons from free space. Compared to photons, surface plasmons exhibit a larger momentum for a given frequency. Thus, a photon incident on a metal surface requires additional lateral momentum for coupling to a surface plasmon. While for single-interface SPPs, this additional momentum can be provided by

Received: July 4, 2023
Revised: October 11, 2023
Accepted: October 12, 2023
Published: November 13, 2023

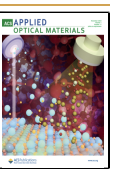

https://doi.org/10.1021/acsaom.3c00228
ACS Appl. Opt. Mater. 2023, 1, 1777−1782

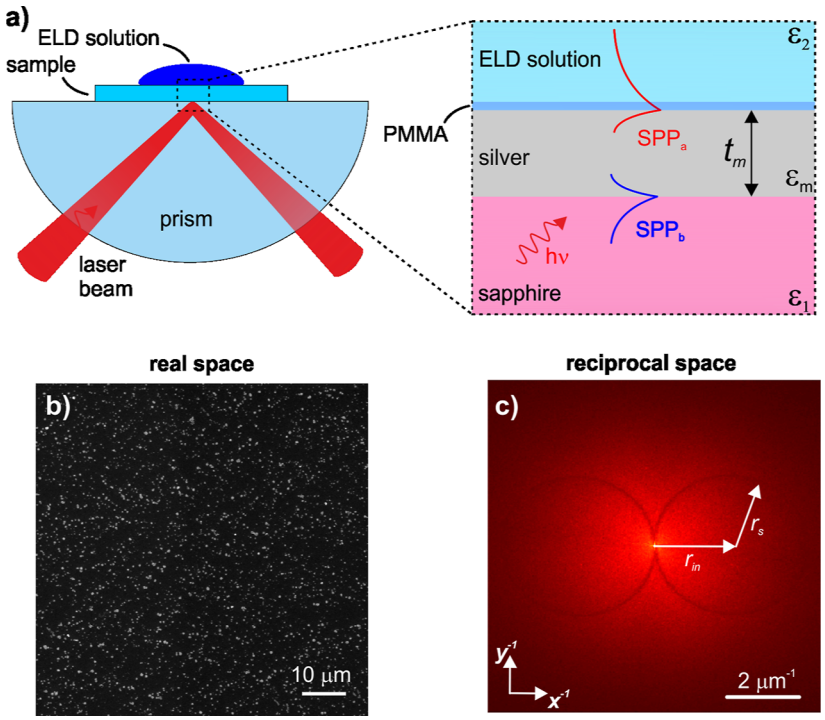

Figure 1. Experimental setup and results of SEM investigations of disorder-engineered metasurfaces fabricated on thick silver films (t_m = 56 nm). (a) Sketch of the Kretschmann−Raether setup used for the experiments and the stack geometry of the samples (inset), emphasizing the two plasmon modes propagating at both interfaces of the silver film (blue and red); (b) typical SEM image of the fabricated metasurfaces; (c) Fourier transform of typical SEM images revealing the engineered disorder of the metasurfaces. The white arrows indicate the horizontal shift r_{in} and the radius r_s of the structure rings.

a high index prism (Kretschmann−Raether geometry), the exploitation of SR-SPPs in ultrathin planar silver films requires surface nanostructures (e.g. gratings) because of the high effective index.[2] The effective index even strongly increases with decreasing t_m.[15] At the same time due to their large field confinement SR-SPPs are extremely sensitive to imperfections like surface roughness.[16] Therefore, the fabrication of nanostructures required for efficient coupling to SR-SPPs becomes even more complex and technologically challenging.

In the scope of sensing, both a spectrally narrow plasmon resonance (high Q-factor) as well as a large spectral shift upon a change in refractive index (sensitivity S) are desired simultaneously to reach satisfying sensing performance. Although SR-SPPs have the opportunity for high sensitivities due to the strong field enhancement, they are spectrally broad due to the short propagation lengths caused by absorption. The nanostructuring of the ultrathin silver film for coupling even causes additional radiation loss, leading to an even broader plasmon resonance.[2]

Recently, it has been shown that a disorder-engineered metasurface consisting of silver nanoparticles (AgNPs) in close proximity to a thin silver film can enable high optical sensing performance.[17] Due to the selective scattering mediated by the metasurface, the SPP modes propagating on the silver film create a sharp resonance in the reflection signal, which is highly sensitive to the refractive index of the analyte. The width of this resonance is around 2 orders of magnitude narrower compared to the initial SPP resonance without the metasurface and is largely governed by the divergence of the laser used for fabrication and probing. It can be concluded from these results that disorder-engineered metasurfaces can enable the generation of high-Q resonances in plasmonic structures, which still exploit the high sensitivity of SPPs resulting in high sensing performance. Following this thought, the ability to address SR-SPPs with their enormous field confinement and sensitivity using such metasurfaces could be an important step toward the detection of single binding events.

In this paper, we demonstrate a method to exploit SR-SPPs in smooth ultrathin silver films using a Kretschmann-Raether geometry and a disorder-engineered metasurface, providing additional momentum. The metasurfaces are fabricated by the plasmon-mediated growth of AgNPs from solution and are inherently adapted to their electromagnetic environment. From the morphology of the metasurface, we show that LR-SPPs and SR-SPPs can be addressed using a laser beam at a fixed incident angle. Further, we analyze the dispersion of both modes with respect to the silver thickness t_m in order to confirm the largely undisturbed propagation of SR-SPPs in the system, which we consider highly promising to increase selectivity and performance in low-cost optical sensors.

2. RESULTS AND DISCUSSION

The experimental setup is shown in Figure 1a. A thin silver film (t_m = 56 nm) on a sapphire substrate is mounted onto a sapphire prism. A p-polarized laser is then aligned with respect to the SPP phase matching conditions. We find the maximum excitation efficiency of SPPs (minimum reflection of the laser) under an incident angle of Θ_{in} = 54° for a laser wavelength of λ_0 = 660 nm. AgNPs are then grown from a solution by electroless deposition (ELD) of silver, as reported previously.[17,18] The resulting plasmonic metasurface is analyzed by scanning electron microscopy (SEM). A typical scanning electron micrograph is shown in Figure 1b. From the SEM investigations, the average particle radius is found to be 87 nm.

https://doi.org/10.1021/acsaom.3c00228
ACS Appl. Opt. Mater. 2023, 1, 1777−1782

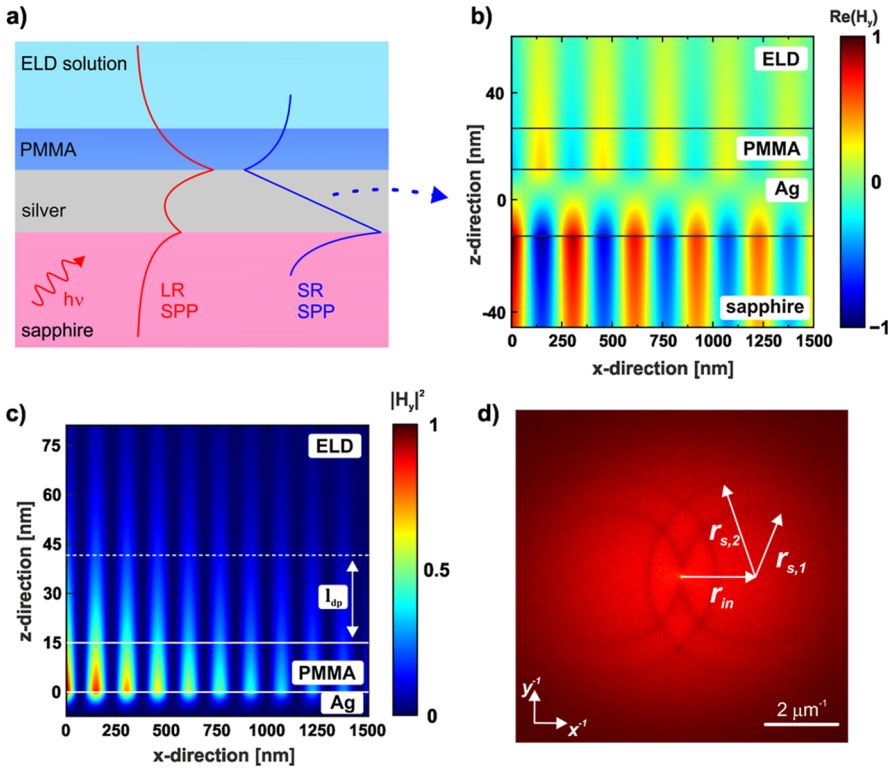

Figure 2. Metasurfaces were deposited on thin silver films (t_m = 25 nm). (a) Layer stack used for the experiments, including qualitative field profiles of LR-SPPs (red) and SR-SPPs (blue); (b) 2D field distribution of the SR-SPP mode simulated using RCWA; (c) corresponding 2D field intensity distribution, including a dashed line indicating the penetration depth of the SR-SPP mode into the ELD solution; (d) typical FTEM of the metasurfaces fabricated on thin silver films exhibiting four structure rings.

Considering the real space, the metasurface appears to contain no deterministic order. However, features of engineered disorder, e.g., disordered hyperuniformity, have recently been found in metasurfaces fabricated with the method presented here.[19] A well-established method to investigate the morphology of metasurfaces is given by the Fourier transform.[20,21] In Figure 1c, a typical Fourier-transformed electron micrograph (FTEM) of the metasurface is shown. Two pronounced dark rings are visible that touch each other at $x^{-1} = y^{-1} = 0$, termed structure rings. As we have shown in previous work, the symmetric shift of the two rings along the x^{-1}-axis r_{in} as well as the radius r_s of the rings (emphasized by white arrows in Figure 1c) can be attributed to the SPP wave involved in the metasurface growth.[17,22] While r_{in} is determined by the incident plane wave, r_s represents the spherical waves scattered by the metasurface. Here, both r_{in} and r_s can be attributed to the SPP_a mode propagating along the silver/ poly(methyl methacrylate) (PMMA) interface as $r_{in} = r_s = 2.14\,\mu m^{-1} = \frac{1}{\lambda_{SPPa}}$. The corresponding effective index of the SPP_a mode is given by $n_{SPPa} = \frac{\lambda_0}{\lambda_{SPPa}} = 1.41$. We did not observe any features of the SPP_b mode. Apparently, it does not interact with the metasurface because of the large silver film thickness.

In the next step, we decreased the silver film thickness to t_m = 25 nm for enabling plasmon hybridization. The resulting layer stacks together with qualitative one-dimensional field profiles of the LR (red) and SR (blue) SPP modes are shown in Figure 2a. In addition, we simulated the two-dimensional field distribution of the SR-SPP mode using rigorous coupled-wave analysis (RCWA). In the RCWA, we used a refractive index for the ELD solution of n_{ELD}, which has been measured using Michelson interferometry in an earlier work.[17] The simulation results are shown in Figure 2b,c displaying the magnetic field distribution and magnetic field intensity. It becomes visible that the SR-SPP mode is predominantly bound to the silver/sapphire interface (see Figure 2b). However, both modes (LR- and SR-SPP) extend into the ELD solution and can thus interact with the later metasurface. Thus, even after the growth of that metasurface, both modes can interact with an analyte placed on top of the device. From the RCWA, we obtained a plasmon wavelength of $\lambda_{SR} = \frac{660nm}{2.13} = 310$ nm for t_m = 25 nm with a corresponding penetration depth (1/e intensity) into the ELD solution (normal to the interface) of 31 nm with respect to the PMMA/ELD interface. We extracted the penetration depth l_{pd} from the simulated mode profiles. Based on a reference intensity at the PMMA/ELD interface (see Figure 2c), the intensity profile of the mode has the proportionality

$$I(z) \propto e^{-z/l_{pd}}$$

The small penetration depth of the SR-SPP into the ELD solution shows the strong field confinement to the metal slab, indicating its promising properties to achieve high surface sensitivities. Thus, the SR-SPPs would be influenced predominantly by surface binding events, and the LR-SPPs would rather detect bulk permittivity fluctuations. In modern optical sensors, this property can be of importance for performance optimization in both bulk and surface refractive index (RI) sensing applications. Recently, the discrimination of bulk and surface RI changes has been realized in fiber-optic sensors supporting photonic modes with different polarization

https://doi.org/10.1021/acsaom.3c00228
ACS Appl. Opt. Mater. 2023, 1, 1777−1782

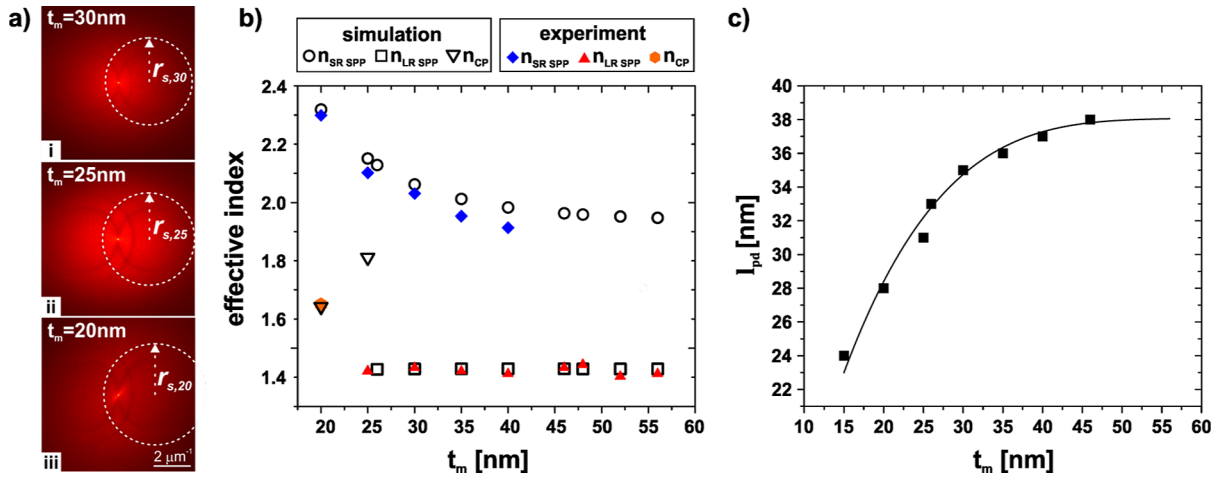

Figure 3. Dispersion of the hybrid plasmonic modes with t_m. (a) FTEMs of metasurfaces fabricated on silver films of 30 nm (i), 25 nm (ii), and 20 nm (iii) thickness; (b) measured and simulated effective indices for LR- and SR-SPPs; (c) simulated penetration depth l_{pd} of SR-SPPs into the ELD solution with respect to t_m. The data points show values for l_{pd} extracted from the mode profiles calculated with a resolution of 1 nm in the z-direction, and the solid line provides visual guidance for the reader.

properties (and different penetration depths).[23,24] Based on the findings in this work, comparable discrimination could be possible using the two hybrid plasmonic modes. In summary, in the simulation, we find two modes with different effective indices that can interact with the growing metasurface.

In the experiment, the reflection of the laser exhibits a minimum at an incident angle of $\Theta_{in} = 54°$ for $\lambda_0 = 660$ nm, and the metasurface is prepared in the same way as reported for the thick silver films. In FTEM, we now observe four instead of two structure rings (see Figure 2d). The inner structure rings again touch each other at $x^{-1} = y^{-1} = 0$. In this case, we found that both the radii and the horizontal shift of the inner structure rings correspond to the LR-SPP mode with $r_{in} = r_{s,1} = 2.16\ \mu m^{-1} = 1/\lambda_{LR}$ and an effective index of 1.42. The radii of the outer structure rings are larger than the horizontal shift ($r_{s,2} > r_{in}$), and thus, these structure rings possess two intersections on the $x^{-1} = 0$ axis. We found that the outer structure rings correspond to the SR-SPP mode as $r_{s,2} = 3.18\ \mu m^{-1} = 1/\lambda_{SR}$.

The shift of the ring centers r_{in} representing the exciting plane wave is identical for both pairs of rings, while the ring radii representing the scattered spherical wave differ. We therefore conclude that in the Kretschmann-Raether configuration, only the LR-SPP can be excited directly. However, the metasurface provides the required momentum to excite SR-SPPs as well, so it mediates coupling between LR-SPPs and SR-SPPs. Thus, it is experimentally proved, that features corresponding to the high index SR-SPP mode ($n_{SR\ SPP} = 2.1$ @ $t_m = 25$ nm) can be incorporated into the resulting metasurface.

The variation of t_m further allows for characterizing the dispersion of the hybrid modes with respect to the thickness of the silver film. We have fabricated silver films with thicknesses ranging from $t_m = 20$ to $t_m = 56$ nm. In Figure 3a, FTEMs of metasurfaces deposited on silver films of three different thicknesses are shown. It becomes visible that the outer structure ring diameter grows with decreasing t_m, while the radius of the inner structure rings stays largely constant in the cases of (i) and (ii). This trend is also valid for larger t_m (see Figure 3b) until hybridization decreases and the hybrid modes segue into SPP_a and SPP_b, whose mode indices are constant over t_m. In our experiments, we could observe hybridization effects up to a silver film thickness of $t_m = 46$ nm. For $t_m = 20$ nm, the effective index of the SR-SPP is as high as 2.3, and according to the simulation, the corresponding penetration depth into the ELD solution is only 28 nm. In Figure 3b, a comparison between the effective indices of the plasmonic modes in simulation and experiment shows that the experimental results fit well with the results of the RCWA. Especially, the good fit considering the effective indices of the SR-SPPs at thin silver thicknesses suggests that the mode propagation is largely undisturbed by the metasurface.

Only for $t_m = 20$ nm, we observed a notable deviation of the simulated effective index of the LR-SPP and the measurement (see Figure 3b). This deviation was reproducible and robust against variations in the surface roughness of the silver. We have confirmed this robustness by comparing silver films deposited using different methods, resulting in a surface roughness of 1.5 nm rms (thermal evaporation) and 1 nm rms (sputtering). The surface roughness has been characterized by atomic force microscopy (see Supporting Figure S1). In Figure 3c, the penetration depth l_{pd} dependent on t_m is shown. In principle, the vertical confinement of the SR-SPP mode would further increase with a decreasing t_m, giving rise to an even higher surface sensitivity. Practically, however, the fabrication of closed silver films with a thickness of only a few nanometers is technologically challenging because of the tendency to form island films dependent on various parameters including temperature, adhesion, and moisture.[25] This can significantly disturb the properties of the plasmonic modes. In fact, we have not observed structure rings in the FTEMs for $t_m < 20$ nm.

In the simulation results, we have found a counter-propagating mode (propagating in $-x$ direction) showing an antisymmetric field profile (see Supporting Information Figure S2) and an effective index of $n_{cp} = 1.64$ (experiment: $n_{cp} = 1.65$). Although this finding suggests that multiple modes, which are accessible by the additional momentum of the metasurface, are involved in the process, a detailed discussion of this mode is beyond the scope of this paper. In the simulation, the expected LR-SPP could not be found for silver films with thicknesses $t_m < 26$ nm. The fact that we have observed features originating from the LR-SPP mode for $t_m =$

https://doi.org/10.1021/acsaom.3c00228
ACS Appl. Opt. Mater. 2023, 1, 1777−1782

25 nm in the experiment (see Figure 3b) can be attributed to the limited measurement accuracy of the profilometer, surface roughness, and permittivity fluctuations, which are not taken into account in the simulation. However, in order to confirm the statement that multiple modes at largely different mode indices and different propagation directions can be involved in the process, we have performed additional experiments, illuminating the samples with two lasers at different wavelengths simultaneously. Figure 4a illustrates the corresponding

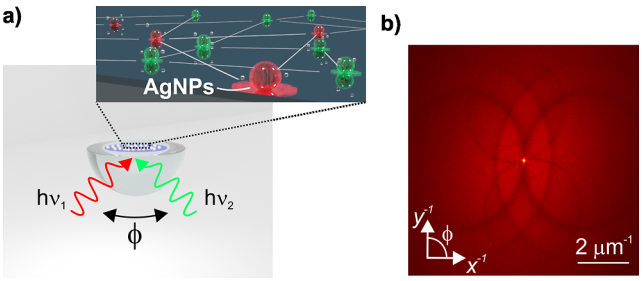

Figure 4. Disorder-engineered metasurfaces fabricated on thin silver films using two excitation lasers simultaneously. (a) Visualization of the experimental setup including the principle of the particle formation under illumination with different light sources (inset); (b) typical FTEM of the resulting metasurface showing eight structure rings corresponding to the four hybrid plasmonic modes involved in the process excited by two lasers at different wavelengths.

experimental setup. Here, we use a spherical plano-convex sapphire lens instead of the half-cylindrical prism to utilize plasmonic modes, which propagate approximately perpendicular to each other ($\varphi \approx 90°$) within the $x-y$ plane. The laser wavelengths are 532 nm (propagating in the x-direction) and 660 nm (propagating in the y-direction).

Considering the FTEM of a metasurface fabricated using two lasers of different wavelengths (see Figure 4b), it becomes clear that also multiple modes with largely different mode indices and different propagation directions in the sample plane can be utilized to incorporate features into the metasurface. In the scope of application, this is of particular interest because it enables us to exploit the functionality of various modes, each having a specific mode profile, penetration depth, effective index, and even frequency at the same spot simultaneously.

3. CONCLUSIONS

The utilization of SR-SPPs in planar silver films has been shown by the plasmon-mediated growth of plasmonic metasurfaces controlled by light. The presented approach offers a facile way to utilize SR-SPPs by using bottom-up fabrication methods of an optical metasurface, while common top-down fabrication methods are often cost-intensive and technologically challenging.

The metasurface provides additional momentum, which enables incorporation of SR-SPP modes in the formation process of the metasurface. We recognize this involvement of SR-SPPs in the metasurface growth because features of these modes (in the form of structure rings) appear in the FTEMs. We find mode indices simulated for planar structures without the metasurface that are in very good agreement with the experiment. This confirms that the metasurface does not significantly disturb the propagation of the present plasmon modes.

The functionality of the metasurface originates from its selective scattering properties, which are highly sensitive to a change in the dielectric environment inside the mode volumes of the LR- and SR-SPP modes. Despite high sensitivities, SR-SPPs usually have limited sensing performance due to comparatively low Q-factors (broad resonance width), owing to short propagation lengths and thus strong localization. However, despite the low Q-factors of the SR-SPPs ranging from $Q = 33$ to $Q = 83$ for $t_m = 20$ nm and $t_m = 40$ nm, respectively, the presented approach enables us to obtain very sharp resonances. The sharpness arises due to the delocalized nature of the system response under coherent illumination on large areas (in the range of several tens of mm^2).[17] The results presented in this work thus represent a first step toward the facile utilization of SR-SPPs in planar optical sensing devices with extraordinary performance in detecting surface binding events in the future. In addition to the implementation of real sensing devices, future steps will also include experiments using other noble metals instead of silver for certain applications. For instance, gold nanoparticles would be a suitable candidate for biological and medical applications due to their high chemical stability and biocompatibility. Furthermore, the synthesis of AgNPs with different shapes, e.g., cubic NPs or pillars, may enable further investigation of the application potential of the presented method.[26]

4. EXPERIMENTAL SECTION

4.1. Sample Preparation

Sapphire substrates with a thickness of $t_s = 500$ μm were used for the experiments. First, an ultrathin chromium adhesion layer ($t_{Cr} = 1.5$ nm) was deposited by sputtering. Then, a silver film was deposited onto the chromium film by physical vapor deposition (thermal evaporation), and a PMMA buffer layer ($t_{PMMA} = 15$ nm) was spin-coated on top of silver, enabling the growth of particles instead of film growth. For the experiments presented in Figure 3, the thickness of the silver films was varied between $t_m = 20$ nm and $t_m = 56$ nm. The film thicknesses were measured using a profilometer. Together with an index matching liquid, the sample was then mounted on a semicylindrical sapphire prism. The excitation of SPPs propagating along the silver/PMMA interface was realized by prism coupling (Kretschmann-Raether configuration) of a p-polarized laser beam ($\lambda_0 = 660$ nm). We found the maximum excitation efficiency of SPPs (minimum in the ATR characteristic) under an incident angle of $\Theta_{in} = 54°$. The AgNPs were then grown from a solution by using the ELD technique. A detailed description of the preparation of the ELD solution for the plasmon-mediated growth of AgNPs can be found in an earlier work.[27] To start the particle growth, the ELD solution was drop cast onto the sample at the position of maximum optical power density ($I_{max} \approx 0.2$ W/cm^2). After around 4 min of deposition (depending on t_m), the laser was switched off, and the ELD solution was removed from the surface. In the last step, AgNPs that had been randomly grown were removed by ultrasonic treatment in a DI-water bath, enabled by their lower surface adhesion.[25]

4.2. Scanning Electron Microscopy

The SEM investigations were conducted using a Philips XL30S FEG system equipped with a field emission cathode.

■ ASSOCIATED CONTENT

Supporting Information

The Supporting Information is available free of charge at https://pubs.acs.org/doi/10.1021/acsaom.3c00228.

AFM images of silver films deposited by different methods and a field plot of the mode solution found at an effective index of 1.64 (PDF)

https://doi.org/10.1021/acsaom.3c00228
ACS Appl. Opt. Mater. 2023, 1, 1777−1782

AUTHOR INFORMATION

Corresponding Author

Patrick Görrn − *Chair of Large Area Optoelectronics, University of Wuppertal, 42119 Wuppertal, Germany; Wuppertal Center for Smart Materials and Systems, University of Wuppertal, 42119 Wuppertal, Germany;* orcid.org/0000-0001-9416-4310; Email: goerrn@uni-wuppertal.de

Authors

Maximilian Buchmüller − *Chair of Large Area Optoelectronics, University of Wuppertal, 42119 Wuppertal, Germany; Wuppertal Center for Smart Materials and Systems, University of Wuppertal, 42119 Wuppertal, Germany*

Ivan Shutsko − *Chair of Large Area Optoelectronics, University of Wuppertal, 42119 Wuppertal, Germany; Wuppertal Center for Smart Materials and Systems, University of Wuppertal, 42119 Wuppertal, Germany*

Sven Oliver Schumacher − *Chair of Large Area Optoelectronics, University of Wuppertal, 42119 Wuppertal, Germany; Wuppertal Center for Smart Materials and Systems, University of Wuppertal, 42119 Wuppertal, Germany*

Complete contact information is available at: https://pubs.acs.org/10.1021/acsaom.3c00228

Notes

The authors declare no competing financial interest.

ACKNOWLEDGMENTS

This project has received funding from the European Research Council (ERC) under the European Union's Horizon 2020 research and innovation program (grant agreement no. 637367) and from the German Federal Ministry of Education and Research (Photonics Research Germany funding program, contract no. 13N15390).

REFERENCES

(1) Maier, S. A. *Plasmonics: Fundamentals And Applications*; Springer Berlin Heidelberg: Berlin, Heidelberg, 2007.

(2) Raether, H. Surface plasmons on smooth surfaces. *Springer Tracts in Modern Physics*; Springer Berlin Heidelberg: Berlin, Heidelberg, 1988; Vol. *111*, pp 4−39.

(3) Gramotnev, D. K.; Bozhevolnyi, S. I. Plasmonics beyond the Diffraction Limit. *Nat. Photonics* **2010**, *4* (2), 83−91.

(4) Nie, S.; Emory, S. R. Probing Single Molecules and Single Nanoparticles by Surface-Enhanced Raman Scattering. *Science* **1997**, *275* (5303), 1102−1106.

(5) Moskovits, M. Surface-Enhanced Raman Spectroscopy: A Brief Retrospective. *J. Raman Spectrosc.* **2005**, *36* (6−7), 485−496.

(6) Shi, J.; Guo, Q.; Shi, Z.; Zhang, S.; Xu, H. Nonlinear Nanophotonics Based on Surface Plasmon Polaritons. *Appl. Phys. Lett.* **2021**, *119* (13), 130501.

(7) Xu, Y.; Bai, P.; Zhou, X.; Akimov, Y.; Png, C. E.; Ang, L.-K.; Knoll, W.; Wu, L. Optical Refractive Index Sensors with Plasmonic and Photonic Structures: Promising and Inconvenient Truth. *Adv. Opt. Mater.* **2019**, *7* (9), 1801433.

(8) Burke, J. J.; Stegeman, G. I.; Tamir, T. Surface-Polariton-like Waves Guided by Thin, Lossy Metal Films. *Phys. Rev. B* **1986**, *33* (8), 5186−5201.

(9) Fan, B.; Liu, F.; Li, Y.; Huang, Y.; Miura, Y.; Ohnishi, D. Refractive Index Sensor Based on Hybrid Coupler with Short-Range Surface Plasmon Polariton and Dielectric Waveguide. *Appl. Phys. Lett.* **2012**, *100* (11), 111108.

(10) Yanai, A.; Levy, U. The Role of Short and Long Range Surface Plasmons for Plasmonic Focusing Applications. *Opt. Express* **2009**, *17* (16), 14270−14280.

(11) Frank, B.; Kahl, P.; Podbiel, D.; Spektor, G.; Orenstein, M.; Fu, L.; Weiss, T.; Horn-von Hoegen, M.; Davis, T. J.; Meyer zu Heringdorf, F. J.; Giessen, H. Short-Range Surface Plasmonics: Localized Electron Emission Dynamics from a 60-Nm Spot on an Atomically Flat Single-Crystalline Gold Surface. *Sci. Adv.* **2017**, *3* (7), No. e1700721.

(12) Tuniz, A.; Chemnitz, M.; Dellith, J.; Weidlich, S.; Schmidt, M. A. Hybrid-Mode-Assisted Long-Distance Excitation of Short-Range Surface Plasmons in a Nanotip-Enhanced Step-Index Fiber. *Nano Lett.* **2017**, *17* (2), 631−637.

(13) Meudt, M.; Bogiadzi, C.; Wrobel, K.; Görrn, P. Hybrid Photonic-Plasmonic Bound States in Continuum for Enhanced Light Manipulation. *Adv. Opt. Mater.* **2020**, *8* (20), 2000898.

(14) Berini, P. Long-Range Surface Plasmon Polaritons. *Adv. Opt. Photon* **2009**, *1* (3), 484−588.

(15) Dionne, J. A.; Sweatlock, L. A.; Atwater, H. A.; Polman, A. Planar Metal Plasmon Waveguides: Frequency-Dependent Dispersion, Propagation, Localization, and Loss beyond the Free Electron Model. *Phys. Rev. B: Condens. Matter Mater. Phys.* **2005**, *72* (7), 075405.

(16) Sukham, J.; Takayama, O.; Lavrinenko, A. V.; Malureanu, R. High-Quality Ultrathin Gold Layers with an APTMS Adhesion for Optimal Performance of Surface Plasmon Polariton-Based Devices. *ACS Appl. Mater. Interfaces* **2017**, *9* (29), 25049−25056.

(17) Shutsko, I.; Buchmüller, M.; Meudt, M.; Görrn, P. Plasmon-Induced Disorder Engineering for Robust Optical Sensors. *Adv. Opt. Mater.* **2022**, *10* (9), 2102783.

(18) Saito, Y.; Wang, J. J.; Smith, D. A.; Batchelder, D. N. A Simple Chemical Method for the Preparation of Silver Surfaces for Efficient SERS. *Langmuir* **2002**, *18* (8), 2959−2961.

(19) Shutsko, I.; Buchmüller, M.; Meudt, M.; Görrn, P. Light-Controlled Fabrication of Disordered Hyperuniform Metasurfaces. *Adv. Mater. Technol.* **2022**, *7* (10), 2200086.

(20) Cabarcos, A.; Paz, C.; Pérez-Orozco, R.; Vence, J. An Image-Processing Algorithm for Morphological Characterisation of Soot Agglomerates from TEM Micrographs: Development and Functional Description. *Powder Technol.* **2022**, *401*, 117275.

(21) Itoh, T.; Yamauchi, N. Surface Morphology Characterization of Pentacene Thin Film and Its Substrate with Under-Layers by Power Spectral Density Using Fast Fourier Transform Algorithms. *Appl. Surf. Sci.* **2007**, *253* (14), 6196−6202.

(22) Polywka, A.; Tückmantel, C.; Görrn, P. Light Controlled Assembly of Silver Nanoparticles. *Sci. Rep.* **2017**, *7* (1), 45144.

(23) Li, Z.; Yang, X.; Wang, F.; Zhu, H.; Jin, X.; Duan, Y.; Chiavaioli, F. Discriminating Bulk and Surface Refractive Index Changes With Fiber-Tip Leaky Mode Resonance. *J. Lightwave Technol.* **2023**, *41* (13), 4341−4351.

(24) Li, Z.; Yang, X.; Zhu, H.; Chiavaioli, F. Sensing Performance of Fiber-Optic Combs Tuned by Nanometric Films: New Insights and Limits. *IEEE Sens. J.* **2021**, *21* (12), 13305−13315.

(25) Polywka, A.; Vereshchaeva, A.; Riedl, T.; Görrn, P. Manipulating the Morphology of Silver Nanoparticles with Local Plasmon-Mediated Control. *Part. Part. Syst. Charact.* **2014**, *31* (3), 342−346.

(26) Khan, Z.; Al-Thabaiti, S. A.; Obaid, A. Y.; Khan, Z. A.; Al-Youbi, A. A. O. Shape-Directing Role of Cetyltrimethylammonium Bromide in the Preparation of Silver Nanoparticles. *J. Colloid Interface Sci.* **2012**, *367* (1), 101−108.

(27) Shutsko, I.; Böttge, C. M.; von Bargen, J.; Henkel, A.; Meudt, M.; Görrn, P. Enhanced Hybrid Optics by Growing Silver Nanoparticles at Local Intensity Hot Spots. *Nanophotonics* **2019**, *8* (9), 1457−1464.